On the Analysis of Spatial Binary Images

Christian Lang[1], Joachim Ohser[2], and Rudolf Hilfer[3]

May 17, 1999

Abstract

This paper deals with the characterization of microscopically heterogeneous, but macroscopically homogeneous spatial structures. A new method is presented which is strictly based on integral-geometric formulae such as Crofton's intersection formulae and Hadwiger's recursive definition of the Euler number. The corresponding algorithms have clear advantages over other techniques. As an example of application we consider the analysis of spatial digital images produced by means of Computer Assisted Tomography.

1 Introduction

Consider a component α of a microstructure which is modeled as a macroscopically homogeneous random set, i.e. the distribution of α is assumed to be invariant with respect to translations. The homogeneity of α allows us to introduce so-called *basic geometric characteristics*: the volume density, the surface density, the specific integral of mean curvature, and the specific integral of total curvature. These quantities play a central role in the quantitative characterization of structures components. Up to multiplicative constants, the geometric characteristics are the densities of the random Minkowski measures defined for a homogeneous random set, and the list of the four geometric characteristics is complete in some sense (cf. Hadwiger's characterization theorem, see e.g. Schneider, 1993, pp. 210f). Procedures for estimating the geometric characteristics are based on Crofton formulae, see Schneider (1993, p. 235), as well as a modification of Hadwiger's recursive definition of the Euler number, see Ohser & Nagel (1996) and Nagel *et al.* (1999).

In recent years, a generalized geometric characterization based on the local volume density, local surface density, and local curvature densities was suggested for the geometric treatment of porous and heterogeneous media in physics, see Hilfer (1991, 1992, 1996). These

[1]Freiberg University of Mining and Technology, Institute of Computer Science, D-09596 Freiberg, Germany

[2]Institute of Industrial Mathematics, Erwin-Schrödinger-Straße, D-67663 Kaiserslautern, Germany

[3]Institute for Computer Applications, University of Stuttgart, Pfaffenwaldring 27, D-70569 Stuttgart, Germany, and Institute of Physics, University of Mainz, D-55099 Mainz, Germany

geometric characteristics can be readily incorporated into the mean field approximation for the microscopic boundary value problems describing transport phenomena in these media. It seems that the resulting parameter-free predictions are in good agreement with experiment, see Widjajakusuma *et al.* (1999).

We assume that the component α is observed in a cuboidal lattice of points, i.e. we consider spatial digital images of the microstructure to be investigated. The discrete version of a (random) set forms a (random) binary digital image. Depending on whether a lattice point is in α or in its complementary set, this point is assigned the Boolean values 1 or 0, respectively. The selection can be performed by thresholding brightness values to separate the α-phase from the background.

For the purpose of application in image analysis, the integrals that occur in the Crofton formulae and Hadwiger's recursive definition are discretized in such a way that "measurement" of the geometric characteristics can be performed by simple "counting" of elements in a digital image where the elements are voxels or neighborhood configurations of voxels. In other words, the observation of the structure in a point lattice implies a corresponding discretization of the integral-geometric formulae. The method which will be used is very close to ordinary *repeated trapezoidal quadrature rule* known from numerical mathematics.

A very powerful technique of image processing is filtering of digital images. However, filtering can also be applied in the image analysis. The statistical estimation of the geometric characteristics suggested in the following includes linear filtering of the binary image as a basic tool. It consists of three steps:

1. Filtering of the binary image which yields a grey-tone image (the "labeling of neighborhood configurations" in the binary image),

2. generating the vector of absolute frequencies of neighborhood configurations (the "integration step"), and

3. estimating the geometric characteristics from the absolute frequencies of configurations (the "analysis step").

By means of filtering, each neighborhood configuration in a binary image is assigned an integer. Thus, the result of the filtering is an image of integer valued voxels, also referred to as a "grey-tone image". The generation of the absolute frequencies of configurations can be understood as a discretized analog of the integration occurring in the integral geometric formulae, and the vector of absolute frequencies carries the "complete information" of the image about the geometric characteristics; it can be used as the data base of statistical estimation. Since the neighborhood configurations are represented by "grey-tones", the vector of absolute frequencies of the neighborhood configuration in the binary image is nothing other than the vector of the absolute frequencies of grey-tones in the filtered image. (This vector will also be referred to as the *grey-tone histogram*.)

2 The Continuous Case: Integral-geometric Formulae

Firstly, we review some integral-geometric formulae widely used in image analysis. We consider a set X of the 3-dimensional space that belongs to the convex ring, i.e. X is a finite union of compact convex sets. Set X can be understood as a particle of a microstructure; functionals of X are commonly referred to as particle parameters. We are interested in the Minkowski functionals of X which are up to multiplicative constants the volume $V(X)$, the surface area $S(X)$, the integral of the mean curvature $M(X)$, and the Euler number $\chi^3(X)$, also referred to as the *connectivity number*. We remark that $K(X) = 4\pi\chi^3(X)$ is the integral of the total curvature of X.

Let E_x denote a plane in space depending on the parameter $x \in I\!R^3$. We introduce spherical polar coordinates $x = (r, \omega)$ where ω represents the normal direction of the plane and r is the distance of the plane from the origin. It is convenient to identify the direction $\omega = (\vartheta, \varphi)$ to be a point on the positive half sphere where $r \in I\!R$ represents the intersection point of the plane E with a straight line orthogonal to E and passing through the origin; define $E_{r,\omega} := E_{-r,-\omega}$ for $r < 0$. The intersection $X \cap E_{r,\omega}$ of a spatial object X and the plane $E_{r,\omega}$ is said to be a 2-dimensional section or a *planar section* of the object X.

A straight line e in the 3-dimensional space can be characterized by the Euler angles $(\phi, \vartheta, \varphi)$ and its distance r from the origin or, alternatively, by the direction $\omega = (\vartheta, \varphi) \in \Omega$ describing the direction of the straight line in the space and the point $y = (r, \phi) \in I\!R^2$ that represents the intersection point of e with a plane $E_{0,\omega}$ orthogonal to e. Thus, we write $e = e_{r,\phi,\vartheta,\varphi}$ or, equivalently $e = e_{y,\omega}$ for a parametric representation of a straight line in 3-dimensional space; $e_{r,\phi,\vartheta,\varphi} := e_{-r,-\phi,\vartheta,\varphi}$ for $r < 0$. The intersection $X \cap e_{y,\omega}$ is said to be a 1-dimensional section or a *linear section* of X. Since X is not necessarily a convex set a linear section of X can consist of a family of chords.

A "0-dimensional section" is obtained when intersecting the set X with a set $\{x\}$ that consists only of the point $x \in I\!R^3$. If the point x is covered by the set X then $X \cap \{x\} = \{x\}$ and, otherwise, this intersection is empty, $X \cap \{x\} = \emptyset$.

By means of Crofton's formulae, the functionals of a 3-dimensional set X are expressed in terms of the functionals defined for lower-dimensional sections. For a 2-dimensional section, let A, L^2, and χ^2 denote the area, the boundary length, and the planar Euler-number, respectively. Notice that $C = 2\pi\chi^2$ is the integral of curvature. (The upper index is used to indicate the dimension of the section where the measurement takes place.) A linear section of the set X can consist of a family of chords; L and χ^1 are their total length and the chord number, respectively. Finally, we introduce the Euler number χ^0 of a 0-dimensional section as $\chi^0(X \cap \{x\}) = 1$ if $x \in X$, and $\chi^0(X \cap \{x\}) = 0$ otherwise. A survey of the Crofton formulae is given in Table 1.

Consider now a pair of parallel section planes $E_{r,\omega}$ and $E_{r+\Delta,\omega}$ having the distance Δ. We give formulae which link the Euler number of a spatial set to functionals of section profiles observed in pairs of parallel sections. Denote $Y_r = (X \cap E_{r,\omega})_{-(r,\omega)}$ the section profiles shifted (or projected) onto the plane $E_{0,\omega}$ where $X_{-(\Delta,\omega)}$ means the translation of X by $-(\Delta, \omega) \in I\!R^3$. The sets Y_r and $Y_{r+\Delta}$ are assigned to the section profiles of X obtained by the intersection

$d=3$		$d=2$		$d=1$		$d=0$
$V(X)$	$=$	$\int A(X \cap E_{r,\omega})\,\mathrm{d}r$	$=$	$\int L(X \cap e_{y,\omega})\,\mathrm{d}y$	$=\int \chi(X \cap \{x\})\,\mathrm{d}x$	
$S(X)$	$=$	$\frac{4}{\pi}\iint L(X \cap E_{r,\omega})\,\mathrm{d}r\,\mu(\mathrm{d}\omega)$	$=4\iint \chi(X \cap e_{y,\omega})\,\mathrm{d}y\,\mu(\mathrm{d}\omega)$			
$M(X)$	$=2\pi\iint \chi(X \cap E_{r,\omega})\,\mathrm{d}r\,\mu(\mathrm{d}\omega)$					
$K(X)$						

Table 1: Survey of the functionals defined for 3-dimensional sets. The measure μ is the normalized Haar measure on the unit sphere, $\mu(\Omega)=1$. By means of Crofton's formulae, these functionals are represented by their counterparts defined on lower dimensional spaces. Notice that $K(X)=4\pi\,\chi(X)$. The innermost integrals are over the orthogonal spaces of $E_{0,\omega}$ and $e_{0,\omega}$, respectively, and the outer integrals are over the unit sphere Ω in $\mathbb{R}^3$. The innermost integral $\wp_V(\omega) := \int \chi(X \cap e_{y,\omega})\mathrm{d}y$ is the specific total projection of α.

with the planes $E_{r,\omega}$ and $E_{r+\Delta,\omega}$; both sets are subsets of the same plane $E_{0,\omega}$, and operations like union or intersection of them are well-defined. Consider a d-dimensional set X belonging to the convex ring. Under certain regularity assumptions made for the set X, Hadwiger's recursive definition of the Euler number can be rewritten as

$$\chi^d(X) = \frac{1}{\Delta}\int \left[\chi^{d-1}\left(Y_r \cup Y_{r+\Delta}\right) - \chi^{d-1}\left(Y_r\right)\right]\,\mathrm{d}r \tag{1}$$

and, equivalently,

$$\chi^d(X) = \frac{1}{\Delta}\int \left[\chi^{d-1}\left(Y_r\right) - \chi^{d-1}\left(Y_r \cap Y_{r+\Delta}\right)\right]\,\mathrm{d}r, \tag{2}$$

see Ohser & Nagel (1996) and Nagel *et al.* (1999), where the integrals are over the orthogonal space of the $d-1$-dimensional hyperplane $E_{r,\omega}$. By means of these recursive formulae, the Euler number χ^d defined on d-dimensional space can be expressed in terms of the Euler number defined on lower-dimensional spaces.

3 Spatial Images and Their Analysis

Turn now to homogeneous structures. Instead of a bounded deterministic set X we will consider a sample of an unbounded random set α which is observed in a bounded spatial window W. We assume that α is homogeneous (i.e. is distribution is invariant with respect to translations). Then it is convenient to estimate the densities of the functionals introduced in the previous section. Our choice for the notation is the same as suggested by the early school of stereology: V_V denotes the volume density of α, S_V is the surface density, and M_V and K_V are the densities of the two curvature measures.

Spatial images of microstructures can be produced by Computer Assisted Tomography (CT scans) and similar techniques using for example X-ray scattering, magnetic resonance, or isotope emission, see Russ (1992, Chapter 7) and Pan *et al.* (1998). Another technique of

formation of 3-dimensional images is by means of an interference confocal scanning microscope under ultrashort pulsed beam illumination, see Gu (1998). One can choose between various types of discretizations of 3-dimensional structures depending on the choice of the spatial lattice where we observe the structure. Examples are the cuboidal lattice, the cubic face centered lattice, and the body centered cubic lattice. Further ideas for spatial lattices which might be useful in image analysis could be taken from crystallography. However, depending on the preferred scanning technique, it is common to use cuboidal lattices, see Fig. 2a, where the unit cell forms a cuboid of edge-lengths Δ_1, Δ_2, and Δ_3. The edge lengths of the unit cell are referred to as the *lattice distances* in the x-, y-, and z-direction, respectively. Their inverses $1/\Delta_1$, $1/\Delta_2$, and $1/\Delta_3$ are said to be the *lateral resolution* with respect to the x-, y-, and z-direction, respectively. The lattice is assumed to be dense, i.e. the lattice distances may be small with respect to the elongation of the objects or features occurring in the α-phase.

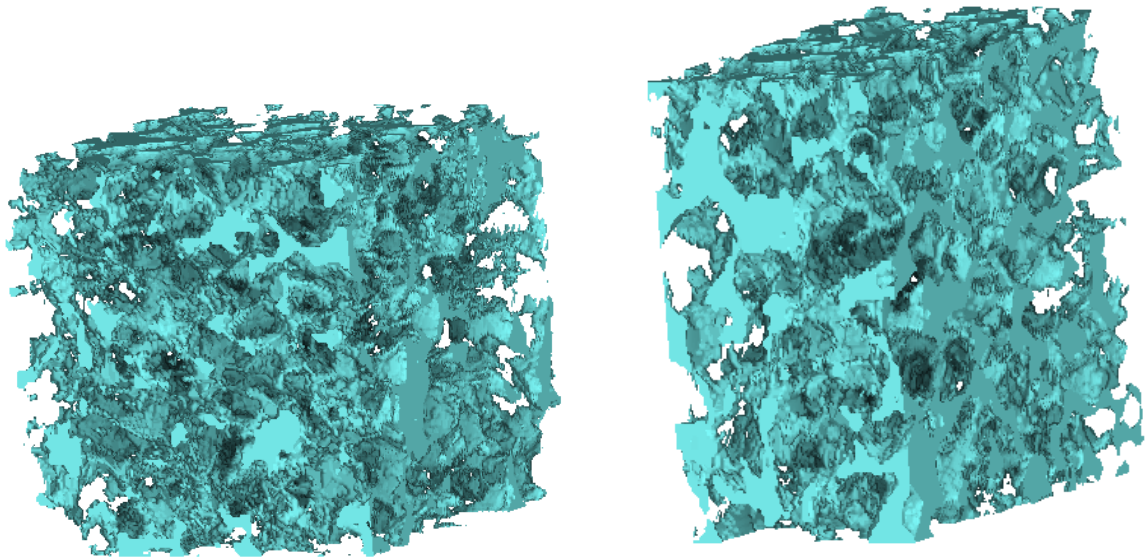

Figure 1: Microstructure of natural sandstone, a) Berea sandstone, b) a weakly consolidated sandstone. In this figure the rock matrix is shown transparent while the pore space is opaque. The 3-dimensional data were obtained by computerized microtomography. The lateral resolution was uniform over all directions; $\Delta = 10\,\mu$m for a) and $\Delta = 30\,\mu$m for b). The determination of the geometric characteristics of these porous media is a prerequisite for studying transport properties such as fluid flow or sound propagation in oil reservoirs, aquifers or other materials, see Biswal *et al.* (1998).

Let a spatial lattice L be given by a sequence $\{x_{ijk},\ i = 0,\dots,n_1,\ j = 0,\dots,n_2,\ k = 0,\dots,n_3\}$ of points $x_{ijk} = (i\Delta_1, j\Delta_2, k\Delta_3)$, see Figure 3a. The spatial window W forms the cuboid $[0, n_1\Delta_1] \times [0, n_2\Delta_2] \times [0, n_3\Delta_3]$ consisting of $n := n_1n_2n_3$ cuboidal cells. As components of the spatial lattice we will consider vertices, edges, and faces of the cells, and the cells of the lattice itself. The cell $[0, \Delta_1] \times [0, \Delta_2] \times [0, \Delta_3]$ is said to be the *unit cell* of

the lattice; its vertices are denoted as shown in Figure 3a.

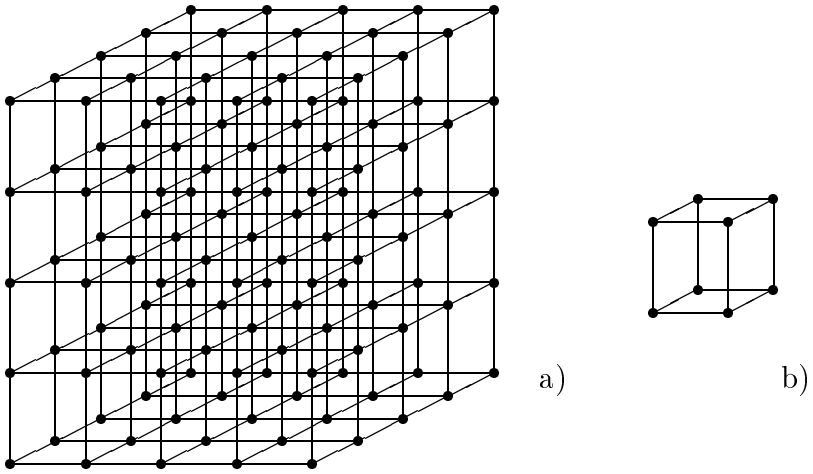

Figure 2: a) A cuboidal lattice L of $5 \times 5 \times 5$ voxels, b) a cell of the lattice. The ordinary cuboidal lattice of uniform lattice distance is the most usual one applied in discretization of spatial microstructures.

The binary image $\alpha \cap L$ can be understood as a matrix $B = (b_{ijk})$ of the components $b_{ijk} = 1_\alpha(x_{ijk})$ where $1_\alpha(x)$ is the indicator function of α. A component b_{ijk} of the binary image is said to be a *voxel*. Surroundings of voxels form image components of higher order, and as the most simple surrounding we consider the $2 \times 2 \times 2$-neighborhood configurations. The $2 \times 2 \times 2$-neighborhood configuration of the voxel b_{ijk} corresponds to the cell assigned to the lattice point x_{ijk}. This neighborhood configuration is assumed to consist of the eight voxels b_{ijk}, $b_{i+1,jk}$, $b_{i,j+1,k}$, $b_{i+1,j+1,k}$, $b_{ij,k+1}$, $b_{i+1,j,k+1}$, $b_{i,j+1,k+1}$, and $b_{i+1,j+1,k+1}$.

3.1 Detection of Neighborhood Configurations

A very simple detection (or coding) of the neighborhood configuration in a binary image can be performed by linear filtering which can be understood as the convolution of the binary image B with a given filter mask F; the result is the grey-tone image $G = B * F$. Since we are interested in the $2 \times 2 \times 2$-neighborhood configurations, we take a filter mask F_1 consisting of eight coefficients f_{ijk}, and if the coefficients are chosen as powers of 2, $f_{ijk} = 2^{i+2j+4k}$, $i, j, k = 0, 1$, see also Figure 3b, then the components g_{ijk} of the grey-tone image G are given by

$$\begin{aligned} g_{ijk} &= b_{ijk} + 2\,b_{i+1,j,k} + 4\,b_{i,j+1,k} + 8\,b_{i+1,j+1,k} \\ &+ 16\,b_{i,j,k+1} + 32\,b_{i+1,j,k+1} + 64\,b_{i,j+1,k+1} + 128\,b_{i+1,j+1,k+1}. \end{aligned}$$

for $i = 0, \ldots, n_1 - 1$, $j = 0, \ldots, n_2 - 1$, and $k = 0, \ldots, n_3 - 1$. An example is given in Figure 3c. The integer g_{ijk} can be understood as the coding of the $2 \times 2 \times 2$-neighborhood configuration of the voxel b_{ijk}. Notice that the function $B \mapsto B * F_1$ is a one-to-one mapping.

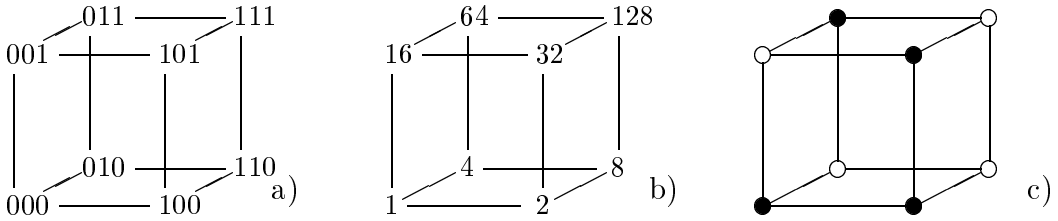

Figure 3: a) The notation used for the vertices of the unit cell, b) spatial representation of the filter mask F_1, c) an example configuration of a $2 \times 2 \times 2$-neighborhood configuration associated with the grey-tone value $g = 99$. The full discs $\bullet$ are assigned to the voxels covered by α whereas the circles $\circ$ are the voxels that hit the complementary phase α^c.

Because of the size of the filter mask F_1, the grey-tone image G has 8 bits per voxel. The linear filtering is free of edge effects if it is restricted to the reduced window $W_1 = [0, (n_1 - 1)\Delta_1] \times [0, (n_2 - 1)\Delta_2] \times [0, (n_3 - 1)\Delta_3]$.

The linear filtering of binary images described above is not original since this kind of coding is used quite often in mathematical morphology. Its use in image processing was first suggested by the Centre de Morphologie Mathématique of the École Nationale Supérieure des Mines de Paris, see Serra (1969).

3.2 The Absolute Frequencies of Configurations

The absolute frequencies of $2 \times 2 \times 2$-neighborhood configuration h_k in the binary image B can be obtained by simply counting the voxels in G which have the grey-tone value g. Let δ be Kronecker's delta, i.e. $\delta_\ell(g) = 1$ for $g = \ell$, and $\delta_\ell(g) = 0$ otherwise. Then

$$h_\ell = \sum_{i=0}^{n_1-1} \sum_{j=0}^{n_2-1} \sum_{j=0}^{n_3-1} \delta_\ell(g_{ijk}), \qquad \ell = 0, \ldots, 255.$$

The function `ghist` computes the grey-tone histogram from a given binary image having $n = n_1 n_2 n_3$ unit cells. It involves linear filtering as well as the generation of the vector h where an explicit computation of the grey-tone image G is avoided. The algorithm is of order $O(n)$; it is linear in the image size.

```
#include<math.h>
#include<malloc.h>

long int *ghist3(int *n, int ***bin_image)
/* given a 3-dimensional binary image bin_image of size n[0..2],
```

```
   the grey-tone histogram h[0..255] of the convolved image is returned
*/
{  int i, j, k;
   int l;
   long int *h;

   h=(long *)malloc(256*sizeof(long));
   for(l=0;l<256;l++) h[l]=0L;
   for(i=0;i<n[0]-1;i++)
      for(j=0;j<n[1]-1;j++)
      {  l=bin_image[i][j][0]+(bin_image[i+1][j][0]<<1)
            +(bin_image[i][j+1][0]<<2)+(bin_image[i+1][j+1][0]<<3);
         for(k=0;k<n[2]-1;k++)
         {  l+=(bin_image[i][j][k+1]<<4)+(bin_image[i+1][j][k+1]<<5)
               +(bin_image[i][j+1][k+1]<<6)+(bin_image[i+1][j+1][k+1]<<7);
            h[l]++; l>>=4;
         }
      }
   return(h);
}
```

The vector $h = (h_k)$ comprises the data for a basic statistical analysis of the α-phase. For example, the total sum of the h_ℓ is simply the cell number n of the lattice, $n = \sum h_\ell$, and thus the volume of the reduced window is obtained from

$$V(W_1) = \Delta_1\Delta_2\Delta_3 \sum_{\ell=0}^{255} h_\ell.$$

Furthermore, from the condensed information about the binary image represented by the vector h, one can estimate the geometric characteristics V_V, S_V, M_V, and K_V as described below.

4 Volume and Volume Density

The volume of α restricted to the window W is usually estimated by the sum of the volumes of those cells for which the (000)-vertices hit α and the other ones are arbitrary (covered by α or its complement α^c). The codes of these configurations are odd, and hence, the sum of the h_ℓ is taken over odd index ℓ,

$$\widehat{V}(\alpha \cap W_1) = \Delta_1\Delta_2\Delta_3 \,\#\Big(\quad\Big) = \Delta_1\Delta_2\Delta_3 \sum_{\ell=0}^{127} h_{2\ell+1},$$

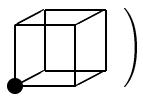

where #() denotes the cardinal number of configurations in the binary image. The full disc • indicates that the (000)-vertex hits α whereas a vacant vertex means that this vertex is covered either by α or by its complement α^c.

From the Crofton formula for the volume, it is immediately clear that $\widehat{V}(\alpha \cap W_1)$ converges to the true value $V(\alpha \cap W_1)$ as the volume of the unit cell converges to 0, $\Delta_1\Delta_2\Delta_3 \to 0$ (and $n_1 n_2 n_3 \to \infty$). Furthermore, since α is assumed to be homogeneous (i.e. the probability measure of α is invariant with respect to Euclidean motion), the estimator

$$\widehat{V_V} = \frac{\sum_{\ell=0}^{127} h_{2\ell+1}}{\sum_{\ell=0}^{255} h_\ell} \tag{3}$$

is unbiased for the volume density.

Now we introduce some *binary bitwise Boolean operators* which are useful to present expressions for estimators of the geometric characteristics. Let $\ell \wedge \kappa$, $\ell \vee \kappa$, and $\neg\kappa$ denote the bitwise "and", the bitwise "or", and the bitwise "not", respectively, of the integers ℓ and κ. The meaning of these operators becomes clear by means of the following examples:

$$\begin{aligned} 88 \wedge 48 &= 01011000\text{b} \wedge 00110000\text{b} = 00010000\text{b} = 16, \\ 88 \vee 48 &= 01011000\text{b} \vee 00110000\text{b} = 01111000\text{b} = 120, \\ \neg 88 &= \neg 01011000\text{b} = 10100111\text{b} = 167. \end{aligned}$$

("b" indicates that the integer is given by its binary representation.) These Boolean operators are equivalent to the *single-character operators* &, |, and $\sim$, respectively, known from the programming language C. It should be noted that the result of the bitwise "not" depends on the number of bits. Furthermore, we remark that the algebraic relationships $\delta_\ell(\ell \vee \kappa) = \delta_\kappa(\ell \wedge \kappa)$ and $\delta_\ell(\ell \wedge \neg\kappa) = \delta_0(\ell \wedge \kappa)$ are valid for any unsigned integers ℓ and κ.

By means of this notation Eq. (3) can be rewritten as

$$\widehat{V_V} = \frac{1}{n}\sum_{\ell=0}^{255} h_\ell\, \delta_\ell(\ell \vee 1) = \frac{1}{n}\sum_{\ell=0}^{255} h_\ell\, [1 - \delta_\ell(\ell \wedge \neg 1)] = \frac{1}{n}\sum_{\ell=0}^{255} h_\ell\, [1 - \delta_0(\ell \wedge 1)].$$

The last equation is the basis of the function `volfrac` which returns an unbiased estimate of the volume fraction when the vector h is input.

```
double volfrac(long int *h)
/* returns an estimate of the volume fraction V_V from the vector h[0..255]
   of absolute frequencies of neighborhood configurations of a binary image
*/
{  int i, j, k, l;
   long int iVol=0L, iVol1=0L;

   for(l=0;l<256;l++){ iVol+=h[l]; if(l==l|1) iVol1+=h[l];}
   return((double)iVol1/(double)iVol);
}
```

Of course, this seems to be a quite complicated estimator for such a simple quantity as the volume fraction. However, the description of this method is very instructive for understanding the method of statistical estimation for other geometric characteristics as well.

5 The Specific Surface Area

The estimation of the specific surface area (which is also referred to as the surface density) is based on the Crofton formula for 1-dimensional sections. For the purpose of application, the edges and the spatial diagonals of the cells are considered to be a system of test segments. In the unit cell, there are 13 segments which correspond to different directions of space: 3 edges, 6 diagonals of the faces, and the 4 spatial diagonals of the cuboid. A survey is given in Table 2. We introduce polar coordinates (r_ν, ω_ν): r_ν and $\omega_\nu = (\vartheta_\nu, \varphi_\nu)$ are the length and direction of the ν-th segment, respectively, and $\Delta_{ij} := \sqrt{(\Delta_i)^2 + (\Delta_j)^2}$ and $\Delta_{123} := \sqrt{(\Delta_1)^2 + (\Delta_2)^2 + (\Delta_3)^2}$ are the lengths of the diagonals of the ij-face and the lengths of the spatial diagonals, respectively.

Test segments	ν	ϑ_ν	φ_ν	r_ν	$\kappa_{0,\nu}$	$\kappa_{1,\nu}$
Cube edges	0	$\pi/2$	0	Δ_1	1	2
	1	$\pi/2$	$\pi/2$	Δ_2	1	4
	2	0	0	Δ_3	1	16
Diagonals	3	$\pi/2$	$\arctan \Delta_2/\Delta_1$	Δ_{12}	1	8
of faces	4	$\pi/2$	$\pi - \arctan \Delta_2/\Delta_1$	Δ_{12}	2	4
	5	$\arctan \Delta_3/\Delta_1$	0	Δ_{13}	1	32
	6	$\arctan \Delta_3/\Delta_1$	π	Δ_{13}	2	16
	7	$\arctan \Delta_3/\Delta_2$	$\pi/2$	Δ_{23}	1	64
	8	$\arctan \Delta_3/\Delta_2$	$3\pi/2$	Δ_{23}	4	16
Spatial	9	$\arctan \Delta_3/\Delta_{12}$	$\arctan \Delta_2/\Delta_1$	Δ_{123}	1	128
diagonals	10	$\arctan \Delta_3/\Delta_{12}$	$\pi - \arctan \Delta_2/\Delta_1$	Δ_{123}	2	64
	11	$\arctan \Delta_3/\Delta_{12}$	$2\pi - \arctan \Delta_2/\Delta_1$	Δ_{123}	4	32
	12	$\arctan \Delta_3/\Delta_{12}$	$\pi + \arctan \Delta_2/\Delta_1$	Δ_{123}	8	16

Table 2: The directions $\omega_\nu = (\vartheta_\nu, \varphi_\nu)$, the lengths r_ν, and the coefficients $\kappa_{0,\nu}$, $\kappa_{1,\nu}$ of the filter mask F_1. The directions ω_ν are points on the positive half-sphere. Estimates of $\wp_V(\omega_\nu)$ for the points $\omega_\nu = -\omega_{\nu-13}$, $\nu = 13, \ldots, 25$, on the negative half-sphere are obtained from (4) when exchanging $\kappa_{0,\nu}$ and $\kappa_{1,\nu}$ but leaving the distances unchanged, $r_\nu = r_{\nu-13}$, $\nu = 13, \ldots, 25$.

For example, the segment $\nu = 9$ formed by the diagonal between the (000)-vertex and the (111)-vertex is of length $r_9 = \Delta_{123}$, and hence, in our lattice the total length of segments corresponding to the direction $\omega_9 = (\vartheta_9, \varphi_9)$ is equal to $n\Delta_{123}$. Consider now the area of the total projection $\wp^9$ of $\alpha \cap W$ with respect to the direction ω_9. An estimator of $\wp^9(\alpha \cap W)$ is obtained from the cardinal number of cells which hit the boundary of α; the (000)-vertices of these cells hit α whereas the (111)-vertices hit the complementary set α^c. Thus, we get

$$\widehat{\wp^9}(\alpha \cap W) = \frac{\Delta_1\Delta_2\Delta_3}{\Delta_{123}} \#\Big(\quad \Big).$$

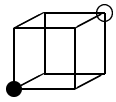

Notice that the ratio $\Delta_1\Delta_2\Delta_3/\Delta_{123}$ is the area of the unit cell of the planar point lattice

obtained by the intersection of the segments of direction ω_9 and a plane perpendicular to these segments. The density of $\wp^9$ – the area of the total projection per unit volume $\wp_V(\omega_9)$ – can be estimated using $\widehat{\wp_V}(\omega_9) = \widehat{\wp^9}(\alpha \cap W)/V(W)$,

$$\widehat{\wp_V}(\omega_9) = \frac{1}{n\,\Delta_{123}} \sum_{\ell=0}^{255} h_\ell\,\delta_\ell(\ell \vee 1)[1 - \delta_\ell(\ell \vee 128)] = \frac{1}{n\,\Delta_{123}} \sum_{\ell=0}^{255} h_\ell\,\delta_\ell(\ell \vee 1)\,\delta_0(\ell \wedge 128).$$

For an arbitrary discrete direction ω_ν, this estimator is of the form

$$\widehat{\wp_V}(\omega_\nu) = \frac{1}{n\,r_\nu} \sum_{\ell=0}^{255} h_\ell\,\delta_\ell(\ell \vee \kappa_{0,\nu})\,\delta_0(\ell \wedge \kappa_{1,\nu}), \quad \nu = 0, \ldots, 25 \tag{4}$$

where $\kappa_{0,\nu}$ and $\kappa_{1,\nu}$ are coefficients of the filter mask F_1. A survey on the quantities used in this estimator is given in Table 2. The estimator (4) is unbiased if α is almost surely morphologically open as well as morphologically closed with respect to a segment of length r_ν and direction ω_ν. Otherwise, if α is almost surely a locally finite union of compact convex sets then it is asymptotically unbiased as $r_\nu \to 0$. Notice that the lateral resolution of the lattice along the test lines is $1/r_\nu$; it is not uniform over all directions.

First, we remark that the estimates of $\wp_V(\omega_\ell)$ have an original meaning in the description of anisotropy of α. Furthermore, from these estimates one obtains an estimate of the specific surface area S_V using

$$\widehat{S_V} = 4 \sum_{\nu=0}^{25} c_\nu\,\widehat{\wp_V}(\omega_\nu). \tag{5}$$

The coefficients c_ν are positive weights satisfying $\sum c_\nu = 1$. The accuracy of estimation is a question of the choice of the weights c_ν which depend on the underlying quadrature rule. Given a direction ω_ν; the weight c_ν depends on the distances between ω_ν and its neighboring directions. One can determine the weights as follows: Divide the unit sphere Ω into the Voronoi cells with respect to the set of directions $\{\omega_\nu,\ \nu = 0, \ldots, 25\}$. Then the obvious choice for c_ν is the relative area of the corresponding Voronoi cell, $4\pi c_\nu$ = "the area of the ν-th Voronoi cell". Clearly, $c_{\nu+13} = c_\nu$. In particular, if the unit cell is a cube (i.e. $\Delta_1 = \Delta_2 = \Delta_3$) then $c_\nu = 0.045\,778$ for $\nu = 0, 1, 2$, $c_\nu = 0.036\,981$ for $\nu = 3, \ldots, 8$, and $c_\nu = 0.035\,196$ for $\nu = 9, \ldots, 12$. These weights have been chosen in the function `specsurf`. Thus, the function `specsurf` returns "accurate" values for the specific surface area S_V only in these cases when the lattice distance is uniform ($\Delta_1 = \Delta_2 = \Delta_3$) or when the component α is isotropic (i.e. its probability is assumed to be invariant with respect to rotations).

Assume a uniform lattice spacing. Because the fineness of discretization of the directions does not depend on the lattice distances, the estimator (5) is normally biased for anisotropic α even as $\Delta_{123} \to 0$. However, if isotropy of α can be assumed then it is asymptotically unbiased as $\Delta_{123} \to 0$, cf. also the discussion in Serra (1982, pp. 220f) and Sandau & Hahn (1993).

```
#include<math.h>

double specsurf(long int *gh, double *Delta)
/* returns the specific surface area S_V from the gray-tone histogram gh[0..255],
   the grid spacing Delta[0..2] is input
*/
{  int kl[13][2]= {{1,2}, {1,4}, {1,16}, {1,8}, {2,4}, {1,32}, {2,16},
     {1,64}, {4,16}, {1,128}, {2,64}, {4,32}, {8,16}};
   double c[13]={0.045778, 0.045778, 0.045778, 0.036981, 0.036981, 0.036981,
      0.036981, 0.036981, 0.036981, 0.035196, 0.035196, 0.035196, 0.035196};
   double S_V=0.0;
   int l, ny;
   long iVil=0L;
   double r[13];

   r[0]=Delta[0]; r[1]=Delta[1]; r[2]=Delta[2];
   r[3]=r[4]=sqrt(Delta[0]*Delta[0]+Delta[1]*Delta[1]);
   r[5]=r[6]=sqrt(Delta[0]*Delta[0]+Delta[2]*Delta[2]);
   r[7]=r[8]=sqrt(Delta[1]*Delta[1]+Delta[2]*Delta[2]);
   r[9]=r[10]=r[11]=r[12]=sqrt(Delta[0]*Delta[0]+Delta[1]*Delta[1]+Delta[2]*Delta[2]);

   for(l=0; l<256; l++)
   {  iVol+=gh[l];
      for(ny=0; ny<13; ny++)
         S_V+=gh[l]*c[ny]/r[ny]*((l==(l|kl[ny][0]))*(0==(l&kl[ny][1]))
                 +(l==(l|kl[ny][1]))*(0==(l&kl[ny][0])));
   }
   return 4.0*S_V/(double)iVol;
}
```

6 The Specific Integral of Mean Curvature

From the Crofton formula for the integral of mean curvature, it immediately follows that the determination of the integral of mean curvature in 3-dimensional space reduces to measurement in 2-dimensional section planes through the specimen. In the cuboidal lattice, there are 13 planes associated with different normal directions and hitting three or four vertices of the cells. The corresponding planar section profiles of the unit cell form rectangles or triangles. Examples are shown in Figure 4, and a survey of all section profiles is given in Table 3.

In the section planes corresponding to the normal directions ω_ν, $\nu = 0, \ldots, 8$, the vertices and edges of the section profiles form a (planar) graph of rectangular cells; for $\nu = 9, \ldots, 12$ the vertices and edges of the section profiles form a triangular graph.

Let $\chi^2(\omega_\nu)$ denote the Euler number corresponding to the normal direction ω_ν of a section plane that hits three or four vertices of a cell. The planar Euler number $\chi^2(\omega_\nu)$ can be estimated by a simple counting of neighborhood configurations. For example, for $\nu = 6$,

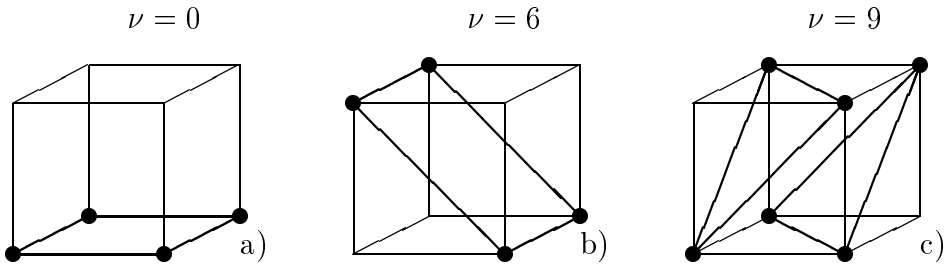

Figure 4: Examples of planar section profiles of the unit cell: a) the rectangle parallel to the xy-plane, b) a rectangular section profile of the unit cell, c) two triangular section profiles of the unit cell pertaining the same normal direction. The vertices and edges of these triangular section profiles of all lattice cells form planar graphs of the type "hexagonal-I", see Serra (1982, p. 174).

Euler's relation implies that

$$\widehat{\chi^2}(\omega_6) = \#\Big(\quad\Big) - \#\Big(\quad\Big) - \#\Big(\quad\Big) + \#\Big(\quad\Big)$$

see Ohser *et al.* (1998). One can easily verify that this formula reduces to

$$\widehat{\chi^2}(\omega_6) = \#\Big(\quad\Big) - \#\Big(\quad\Big) + \#\Big(\quad\Big).$$

A further simplification arises if we add the spatial diagonal between the (100)-vertex and the (011)-vertex (a diagonal of the section rectangle). Then the rectangular unit cell of the planar graph under consideration is tessellated into two triangles and the last term of the previous equation vanishes, so the Euler number for the modified planar graph can be estimated using

$$\widetilde{\chi^2}(\omega_6) = \#\Big(\quad\Big) - \#\Big(\quad\Big).$$

Let a_6 denote the area of the rectangular cell; then the density estimator of the Euler number is $\widetilde{\chi_A}(\omega_6) = \widetilde{\chi^2}(\omega_6)/a_6$ and thus

$$\begin{aligned}\widetilde{\chi_A}(\omega_6) \;=\; & \frac{1}{n\,a_6}\Bigg[\sum_{\ell=0}^{255} h_\ell\,\delta_\ell(\ell\vee 2)\,\delta_0(\ell\wedge 8)\,\delta_0(\ell\wedge 16)\,\delta_0(\ell\wedge 64) \\ & \qquad - \sum_{\ell=0}^{255} h_\ell\,\delta_\ell(\ell\vee 2)\,\delta_\ell(\ell\vee 8)\,\delta_\ell(\ell\vee 16)\,\delta_0(\ell\wedge 64)\Bigg]\end{aligned}$$

In the general case we obtain for the rectangular section profiles of the unit cell

$$\widetilde{\chi_A}(\omega_\nu) \;=\; \frac{1}{n\,a_\nu}\Bigg[\sum_{\ell=0}^{255} h_\ell\,\delta_\ell(\ell\vee\kappa_{0,\nu})\,\delta_0(\ell\wedge\kappa_{1,\nu})\,\delta_0(\ell\wedge\kappa_{2,\nu})\,\delta_0(\ell\wedge\kappa_{3,\nu})$$

$$- \sum_{\ell=0}^{255} h_\ell \, \delta_\ell(\ell \vee \kappa_{0,\nu}) \, \delta_\ell(\ell \vee \kappa_{1,\nu}) \, \delta_\ell(\ell \vee \kappa_{2,\nu}) \, \delta_0(\ell \wedge \kappa_{3,\nu}) \Bigg], \tag{6}$$

$\nu = 0, \ldots, 8$, where $\kappa_{0,\nu}$, $\kappa_{1,\nu}$, $\kappa_{2,\nu}$, and $\kappa_{3,\nu}$ are the coefficients of the filter mask F_1 relating to the vertices of the rectangular section profiles. For the triangular section profiles

$$\begin{aligned} \widehat{\chi_A}(\omega_\nu) \;=\; & \frac{1}{n\, a_\nu} \Bigg[\sum_{\ell=0}^{255} h_\ell \, \delta_\ell(\ell \vee \kappa_{0,\nu}) \, \delta_0(\ell \wedge \kappa_{1,\nu}) \, \delta_0(\ell \wedge \kappa_{2,\nu}) \\ & - \sum_{\ell=0}^{255} h_\ell \, \delta_\ell(\ell \vee \kappa_{0,\nu+13}) \, \delta_\ell(\ell \vee \kappa_{1,\nu+13}) \, \delta_(\ell \wedge \kappa_{2,\nu+13}) \Bigg], \end{aligned} \tag{7}$$

$\nu = 9, \ldots, 12$, cf. Serra (1982, p. 233). The constants used in these formulae are given in Table 3 where A_{123} denotes the area of the triangles, $A_{123} = \sqrt{s(s-\Delta_{12})(s-\Delta_{13})(s-\Delta_{23})}$ with $s = (\Delta_{12} + \Delta_{13} + \Delta_{23})/2$ (Heron formula); the constants θ_{12} and θ_{123} are the azimuth angle and the zenith angle of the normal direction of the section triangles, respectively, $\theta_{12} = \operatorname{arccot}(\Delta_2/\Delta_1)$ and $\theta_{123} = \arcsin[(\Delta_{12}\Delta_3)/(4A_{123})]$. The coefficients $\kappa_{0,\nu}$, $\kappa_{1,\nu}$, $\kappa_{2,\nu}$, and $\kappa_{3,\nu}$ are associated with the vertices of the section polygons and the directions ω_ν are points on the positive half-sphere.

Test areas	ν	ϑ_ν	φ_ν	a_ν	$\kappa_{0,\nu}$	$\kappa_{1,\nu}$	$\kappa_{2,\nu}$	$\kappa_{3,\nu}$
Faces	0	0	0	$\Delta_1\Delta_2$	1	2	4	8
of the cuboid	1	$\pi/2$	$\pi/2$	$\Delta_1\Delta_3$	1	2	16	32
	2	$\pi/2$	0	$\Delta_2\Delta_3$	1	4	16	64
Diagonal	3	$\operatorname{arccot}\Delta_3/\Delta_2$	$3\pi/2$	$\Delta_3\Delta_{12}$	1	2	64	128
rectangles	4	$\operatorname{arccot}\Delta_3/\Delta_2$	$\pi/2$	$\Delta_3\Delta_{12}$	4	16	8	32
	5	$\operatorname{arccot}\Delta_3/\Delta_1$	π	$\Delta_2\Delta_{13}$	1	32	4	128
	6	$\operatorname{arccot}\Delta_3/\Delta_1$	0	$\Delta_2\Delta_{13}$	2	8	16	64
	7	$\pi/2$	θ_{12}	$\Delta_1\Delta_{23}$	2	4	32	64
	8	$\pi/2$	$\pi - \theta_{12}$	$\Delta_1\Delta_{23}$	1	16	8	128
Diagonal	9	θ_{123}	$\pi + \theta_{12}$	$2A_{123}$	1	64	32	–
triangles	10	θ_{123}	$2\pi - \theta_{12}$	$2A_{123}$	2	16	128	–
	11	θ_{123}	θ_{12}	$2A_{123}$	8	64	32	–
	12	θ_{123}	$\pi - \theta_{12}$	$2A_{123}$	4	16	128	–
	22	$\pi/2 + \theta_{123}$	θ_{12}	$2A_{123}$	2	4	128	–
	23	$\pi/2 + \theta_{123}$	$\pi - \theta_{12}$	$2A_{123}$	8	1	64	–
	24	$\pi/2 + \theta_{123}$	$\pi + \theta_{12}$	$2A_{123}$	2	4	16	–
	25	$\pi/2 + \theta_{123}$	$2\pi - \theta_{12}$	$2A_{123}$	8	1	32	–

Table 3: The directions $\omega_\nu = (\vartheta_\nu, \varphi_\nu)$, the areas a_ν, and coefficients $\kappa_{0,\nu}$, $\kappa_{1,\nu}$, $\kappa_{2,\nu}$, $\kappa_{3,\nu}$ of the filter mask F_1. Notice that for $\nu = 13, \ldots, 21$ the constants can be obtained from $\vartheta_\nu = \vartheta_{\nu-13}$, $\varphi_\nu = -\varphi_{\nu-13}$, $\kappa_{0,\nu} = \kappa_{3,\nu-13}$, $\kappa_{1,\nu} = \kappa_{2,\nu-13}$, $\kappa_{2,\nu} = \kappa_{1,\nu-13}$, $\kappa_{3,\nu} = \kappa_{0,\nu-13}$, and $a_\nu = a_{\nu-13}$.

We firstly refer to the meaning of the estimates $\widehat{\chi_A}(\omega_\nu)$ in the characterization of structural

anisotropy. Furthermore, as a discrete version of Crofton's formula one obtains from the $\widehat{\chi_A}(\omega_\nu)$ an estimator of the specific integral of mean curvature,

$$\widehat{M_V} = 2\pi \sum_{\nu=0}^{25} c_\nu \, \widehat{\chi_A}(\omega_\nu) \tag{8}$$

where the c_ν are suitable positive weights satisfying $\sum c_\nu = 1$, cf. also the discussion in the previous section. The weights used in the function `specimc` correspond to a uniform lattice spacing.

```
#include<math.h>

double specimc(long int *gh, double *Delta)
/* returns the specific integral of mean curvature M_V from the gray-tone
   histogram gh[0..255], the grid spacing Delta[0..2] is input
*/
{  int kr[9][4]={{1,2,4,8}, {1,2,16,32}, {1,4,16,64}, {1,2,64,128},
      {4,16,8,32}, {1,32,4,128}, {2,8,16,64}, {2,4,32,64}, {1,16,8,128}};
   int kt[8][3]={{1,64,32}, {2,16,128}, {8,64,32}, {4,16,128},
      {2,4,128}, {8,1,64}, {2,4,16}, {8,1,32}};
   double c[13]={0.045778, 0.045778, 0.045778, 0.036981, 0.036981, 0.036981,
      0.036981, 0.036981, 0.036981, 0.035196, 0.035196, 0.035196, 0.035196};
   double delta01 = sqrt(Delta[0]*Delta[0]+Delta[1]*Delta[1]);
   double delta02 = sqrt(Delta[0]*Delta[0]+Delta[2]*Delta[2]);
   double delta12 = sqrt(Delta[1]*Delta[1]+Delta[2]*Delta[2]);
   double s=(delta01+delta02+delta12)/2;
   double a[13], M_V=0.0;
   int ir, l, ny;
   long iVol=0L;

   a[0]=Delta[0]*Delta[1]; a[1]=Delta[0]*Delta[2];
   a[2]=Delta[1]*Delta[2];a[3]=a[4]=Delta[2]*delta01;
   a[5]=a[6]=Delta[1]*delta02; a[7]=a[8]=Delta[0]*delta12;
   a[9]=a[10]=a[11]=a[12]=2*sqrt(s*(s-delta01)*(s-delta02)*(s-delta12));
   for(l=0; l<256; l++)
   {  iVol+=gh[l];
      for(ny=0; ny<9; ny++)
         for(ir=0; ir<4; ir++)
            M_V+=(double)gh[l]*c[ny]/(4.0*a[ny])
                 *((l==(l|kr[ny][ir]))*(0==(l&kr[ny][(ir+1)%4]))
                 *(0==(l&kr[ny][(ir+2)%4]))*(0==(l&kr[ny][(ir+3)%4]))
                 -(l==(l|kr[ny][ir]))*(l==(l|kr[ny][(ir+1)%4]))
                 *(l==(l|kr[ny][(ir+2)%4]))*(0==(l&kr[ny][(ir+3)%4])));
      for(ny=9; ny<13; ny++)
         for(ir=0; ir<3; ir++)
            M_V+=(double)gh[l]*c[ny]/(3.0*a[ny])
                  *((l==(l|kt[ny-9][ir]))*(0==(l&kt[ny-9][(ir+1)%3]))
                  *(0==(l&kt[ny-9][(ir+2)%3]))
                  -(l==(l|kt[ny-5][ir]))*(l==(l|kt[ny-5][(ir+1)%3]))
                  *(0==(l&kt[ny-5][(ir+2)%3])));
   }
```

```
   return 4.0*M_PI*M_V/(double)iVol;
}
```

7 The Specific Integral of Total Curvature

An estimator of the Euler number χ of α restricted to the window W can be written as the scalar product of the vector h of absolute frequencies of $2\times2\times2$-neighborhood configurations and a vector u that consists of the integers $-2,\ -1,\ 0$, and 1, $\widehat{\chi}(\alpha\cap W) = \langle h,u\rangle = \sum_{\ell=0}^{255} h_\ell u_\ell$. The coefficients u_ℓ of u are obtained from a threefold application of the modification of Hadwiger's recursive definition of the Euler number; the coefficients are listed in the function `specenb`. We remark that, basing on a graph-theoretical approach, Serra found a quite similar formula for the Euler number, see Serra (1969) and Serra (1982, p. 204).

For the density χ_V of the Euler number we obtain the estimator

$$\widehat{\chi_V} = \frac{\langle h,u\rangle}{n\,\Delta_1\Delta_2\Delta_3}.$$

This estimator is unbiased estimator if α satisfies certain regularity condition, see Nagel *et al.* (1999).

```
#include<math.h>

double specenb(long int *h, double *Delta)
/* returns the specific Euler numver chi_V from the vector h[0..255]
   of absolute freqencies, the lattice distances Delta[0..2] are input
*/
{  int i, j, l;
   long int iChi=0L, iVol=0L;
   int iu[256]=
   {   0, 0, 0, 0, 0, 0, 0, 0, 0, 0, 0, 0, 0, 0, 0, 0,  //   0.. 15
       0, 0, 0, 0, 0, 0, 1, 0, 0, 0, 0, 0, 0, 0, 1, 0,  //  16.. 31
       0, 0, 0, 0,-1, 0, 0, 0,-1, 0, 0, 0,-1, 0, 0, 0,  //  32.. 47
       0, 0, 0, 0, 0, 0, 1, 0,-1, 0, 0, 0, 0, 0, 1, 0,  //  48.. 63
       0, 0,-1, 0, 0, 0, 0, 0,-1, 0,-1, 0, 0, 0, 0, 0,  //  64.. 79
       0, 0, 0, 0, 0, 0, 1, 0,-1, 0, 0, 0, 0, 0, 1, 0,  //  80.. 95
      -1, 0,-1, 0,-1, 0, 0, 0,-2, 0,-1, 0,-1, 0, 0, 0,  //  96..111
       0, 0, 0, 0, 0, 0, 1, 0,-1, 0, 0, 0, 0, 0, 1, 0,  // 112..127
       1, 0, 0, 0, 0, 0, 0, 0, 0, 0, 0, 0, 0, 0, 0, 0,  // 128..143
       0, 0, 0, 0, 0, 0, 1, 0, 0, 0, 0, 0, 0, 0, 1, 0,  // 144..159
       0, 0, 0, 0,-1, 0, 0, 0,-1, 0, 0, 0,-1, 0, 0, 0,  // 160..175
       0, 0, 0, 0, 0, 0, 1, 0,-1, 0, 0, 0, 0, 0, 1, 0,  // 176..191
       0, 0,-1, 0, 0, 0, 0, 0,-1, 0,-1, 0, 0, 0, 0, 0,  // 192..207
       0, 0, 0, 0, 0, 0, 1, 0,-1, 0, 0, 0, 0, 0, 1, 0,  // 208..223
      -1, 0,-1, 0,-1, 0, 0, 0,-2, 0,-1, 0,-1, 0, 0, 0,  // 224..239
       0, 0, 0, 0, 0, 0, 1, 0,-1, 0, 0, 0, 0, 0, 1, 0   // 240..255
   };
   for(l=0;l<256;l++){  iChi+=iu[l]*h[l]; iVol+=h[l];}
```

```
   return (double)iChi/((double)iVol*Delta[0]*Delta[1]*Delta[2]);
}
```

Because of edge effects, estimates of χ_V depend on "direction of measurement"; estimates returned by the function `specenb` are assigned to the z-direction. Under some weak assumptions made for α the estimator $\widehat{\chi_V}$ is unbiased. However, from a statistical point of view estimates of χ_V should be averaged over "all possible directions". For this reason we also introduce an estimator of the specific integral of the total curvature K_V which does not have this disadvantage.

Given a cube centered at the origin, we consider those rotations ω of the proper rotation group which keep this cube unchanged. There are 24 rotations ω_ν and the symmetry group $\{\omega_0, \ldots, \omega_{23}\}$ of the cube is also referred to as the *octaeder group*. Denote $\widehat{\chi_V}(\omega_\nu)$ the estimator of χ_V which is assigned to the rotation ω_ν. Then the specific integral of total curvature K_V can be estimated using

$$\widehat{K_V} = 4\pi \sum_{\nu=0}^{23} c_\nu \, \widehat{\chi_V}(\omega_\nu)$$

where the weights c_ν are chosen as $c_\nu = 1/24,\ \nu = 0, \ldots, 23$. One can easily see that this estimator can be rewritten as $\widehat{K_V} = (\pi/6)\langle h, v\rangle/(n\Delta_1\Delta_2\Delta_3)$ for a suitable chosen vector v. The simplicity of this estimator is reflected by the very short source code of the function `specitc` presented below.

```
#include<math.h>

double specitc(long int *h, double *Delta)
/* returns the specific integral of total curvature K_V from the vector h[0..255]
   of absolute freqencies, the lattice distances Delta[0..2] are input
*/
{  int i, j, l;
   long int iChi=0L, iVol=0L;
   int iv[256]=
   {  0,  3,  3,  0,  3,  0, -6, -3,  3, -6,  0, -3,  0, -3, -3,  0,   //   0.. 15
      3,  0, -6, -3, -6, -3, -3, -6,-12, -8, -8, -6, -8, -6,  0, -3,   //  16.. 31
      3, -6,  0, -3,-12, -8, -8, -6, -6, -3, -3, -6, -8,  0, -6, -3,   //  32.. 47
      0, -3, -3,  0, -8, -6,  0, -3, -8,  0, -6, -3,  0,  3,  3,  0,   //  48.. 63
      3, -6,-12, -8,  0, -3, -8, -6, -6, -3, -8,  0, -3, -6, -6, -3,   //  64.. 79
      0, -3, -8, -6, -3,  0,  0, -3, -8,  0,  0,  3, -6, -3,  3,  0,   //  80.. 95
     -6, -3, -8,  0, -8,  0,  0,  3, -3, 12,  0,  9,  0,  9,  3,  6,   //  96..111
     -3, -6, -6, -3, -6, -3,  3,  0,  0,  9,  3,  6,  3,  6,  6,  3,   // 112..127
      3,-12, -6, -8, -6, -8, -3,  0,  0, -8, -3, -6, -3, -6, -6, -3,   // 128..143
     -6, -8, -3,  0, -3,  0, 12,  9, -8,  0,  0,  3,  0,  3,  9,  6,   // 144..159
      0, -8, -3, -6, -8,  0,  0,  3, -3,  0,  0, -3, -6,  3, -3,  0,   // 160..175
     -3, -6, -6, -3,  0,  3,  9,  6, -6,  3, -3,  0,  3,  6,  6,  3,   // 176..191
      0, -8, -8,  0, -3, -6,  0,  3, -3,  0, -6,  3,  0, -3, -3,  0,   // 192..207
     -3, -6,  0,  3, -6, -3,  9,  6, -6,  3,  3,  6, -3,  0,  6,  3,   // 208..223
     -3,  0, -6,  3, -6,  3,  3,  6, -6,  9, -3,  6, -3,  6,  0,  3,   // 224..239
      0, -3, -3,  0, -3,  0,  6,  3, -3,  6,  0,  3,  0,  3,  3,  0    // 240..255
```

```
    };
    for(l=0;l<256;l++){  iChi+=iv[l]*h[l]; iVol+=h[l];}
    return M_PI/6.*(double)iChi/((double)iVol*Delta[0]*Delta[1]*Delta[2]);
}
```

8 Results and Concluding Remarks

The images shown in Figure 2 were given in form of 3-dimensional matrices. There was an uniform lattice distance, $\Delta := \Delta_1 = \Delta_2 = \Delta_3$. A survey of the results is given in Table 4.

	Berea	weakly consolidated
voxels	$128 \times 128 \times 128$	$128 \times 128 \times 73$
Δ	$10\,\mu$m	$30\,\mu$m
$V(W_1)$	$2.048\,\mathrm{mm}^3$	$31.4\,\mathrm{mm}^3$
V_V	82.2 %	75.3 %
S_V	$13.859\,\mathrm{mm}^{-1}$	$5.908\,\mathrm{mm}^{-1}$
M_V	$-252\,\mathrm{mm}^{-2}$	$-25.3\,\mathrm{mm}^{-2}$
K_V	$2\,164\,\mathrm{mm}^{-3}$	$-324\,\mathrm{mm}^{-3}$

Table 4: A survey of the densities of the random Minkowski measures for the specimens shown in Figures 2a and 2b. The volume fraction is that of the rock matrix α while the volume fraction of the pore space α^c is $1 - V_V$. Furthermore, we remark that $S_V(\alpha) = S_V(\alpha^c)$, $M_V(\alpha) = -M_V(\alpha^c)$, and $K_V(\alpha) = K_V(\alpha^c)$.

It is possible to fit a Boolean model to the rock phase: the rock phase can be described by a locally countable union of convex bodies having random size and shape where the body centers form a spatial Poissonian point field. Some of the model parameters – the point density and the expectations of the Minkowski functionals of the typical body – can be adapted to the measured values. When applying Miles' famous formulas

$$\begin{aligned} V_V &= 1 - \exp\{-\lambda\overline{V}\}, \\ S_V &= \lambda\overline{S}\,\exp\{-\lambda\overline{V}\}, \\ M_V &= \left[2\pi\lambda\overline{\overline{b}} - \frac{(\pi\lambda\overline{S})^2}{32}\right]\exp\{-\lambda\overline{V}\}, \\ K_V &= \left[4\pi\lambda - 2\pi\,\lambda^2\overline{S}\,\overline{\overline{b}} + \frac{(\pi\lambda\overline{S})^3}{24}\right]\exp\{-\lambda\overline{V}\}, \end{aligned}$$

see Miles (1976), one obtains for the Berea sandstone the point density $\lambda = 1.281 \cdot 10^{-7}$, the mean volume $\overline{V} = 1.529 \cdot 10^6\,\mu\mathrm{m}^3$, the mean surface area $\overline{S} = 1.316 \cdot 10^5\,\mu\mathrm{m}^2$, and the mean caliper diameter $\overline{\overline{b}} = 2.720 \cdot 10^2\,\mu$m. However, the computation of λ, $\overline{V}$, $\overline{S}$, and $\overline{\overline{b}}$ from estimates of V_V, S_V, M_V, and K_V is very sensitive with respect to errors in the estimates as well as deviations of the structure from the model assumption. For the weakly consolidated sandstone we would obtain a negative point density λ.

The surface of α observed in a cuboidal lattice can be modeled as smoth spatial surface which separates the set of lattice points covered by α from the complementary set of lattice points. Modelling such a surface is a real problem which can be solved by techniques well-known from computer graphics. Anyway, given such a smooth surface then a straightforward algorithm for computing the surface area as well as the two curvature integrals could be based on conventional intergration over this surface, see e.g. Cohen-Or. & Kaufman (1995).

The technique presented in this paper is quite different from this approach. Due to Crofton's intersection formulae and Hadwiger's recursive definition of the Euler number, we are able to estimate the surface area and the two curvature integrals without having to localize the surface, and hence, we do not need any model for the surface. Our technique is related to the method of estimating the specific surface from the correlation function, as first discussed by Debye (1957). However, our technique does not evaluate the full correlation function, and it involves a filtering that is normally not used when calculating correlation functions. Furthermore, our method is faster and more efficient. The problem reduces to the numerical integration of functions defined on the unit sphere. For both approaches the accuracy of estimation depends on the numerical accuracy of integration (i.e. it depends on the chosen quadrature rule). However, our approach leads to algorithms which are much simpler and more efficient than those based on the conventional technique.

The length of the vector of absolute frequencies is equal to the total number of different configurations occurring in the binary image. Hence, the vector length does not depend on the image size itself, it depends only on the size of the applied filter mask. This is a clear advantage over other techniques of image analysis, in particular, for large spatial images or when data have to be accumulated from a series of images of the same specimen but of different sizes. Hence, the "analysis step" can be performed very easily and quickly, and the algorithm for the statistical estimation of the geometric characteristics can be presented in a well-structured form.

The size of the filter mask F can be increased. Then, usually the angular resolution is improved while the lateral resolution is reduced. In other words, by means of the size of the filter mask one can choose between high digital resolution or high directional resolution. The errors corresponding to the lateral resolution and the directional resolution, respectively, behave in an opposite way. The optimal size of F depends on the "regularity of the surface" of α as well as on the "degree of anisotropy", cf. the discussion in Ohser *et al.* (1998).

Depending on the size of the corresponding filter mask, the amounts of memory space for the obtained grey-tone image as well as the grey-tone histogram can become very large. Therefore, in the implementation of the algorithms for larger filter masks, the explicit representation of the grey-tone image G and the grey-tone histogram h should be avoided.

Acknowledgement. One of us (R. H.) is grateful to the Deutsche Forschungsgemeinschaft for financial support.

References

Biswal, B., C. Manwart, and R. Hilfer (1998) Three-dimensional local porosity analysis of porous media. *Physika* **A 255**, 221-241.

Cohen-Or, D., and A. Kaufman (1995) Fundamentals of surface voxelization. *Graphical Models and Image Processing* **57**, 453–461.

Debye, P, H.R. Anderson, and H. Brumberger (1957) Scattering by an inhomogeneous solid II: The correlation function and its application. *J. Appl. Phys.* **28**, 679–683.

Gu, M. (1998) Image formation in femtosecond confocal interference microscopy. *Microscopy and Microanalysis* **4**, 63–71.

Hilfer, R. (1992) Geometric and dielectric characterization of porous media. *Phys. Rev.* **B44**, 60–.

Hilfer, R. (1992) Local porosity theory for flow in porous media. *Phys. Rev.* **B45**, 7115–.

Hilfer, R. (1996) Transport and relaxation phenomena in porous media. *Adv. Chem. Phys.* **XCII**, 299–.

Nagel, W., J. Ohser, and K. Pischang (1999) An integral-geometric approach for the EulerPoincaré characteristic of spatial images. *J. Microscopy* .

Ohser, J., and W. Nagel (1996) The estimation of the Euler-Poincaré characteristic from observations on parallel sections. *J. Microscopy* **184**, S. 117–126.

Ohser, J., B. Steinbach, and C. Lang (1998) Efficient texture analysis of binary images. *J. Microscopy* **192**, 20–28.

Miles, R. (1976) Estimating aggregate and overall characteristics from thick sections by transmission microscopy. *J. Microscopy* **107**, 227–233.

Pan, S., W. Liou, A. Shih, M.-S. Park, G. Wang, S. P. Newberry, H. Kim, D. M. Shinozaki, P.-C. Cheng (1998) Experimental system for X-ray cone-beam microtomography. *Microscopy and Microanalysis* **4**, 56–62.

Russ, J. C. (1992) *The Image Processing Handbook.* CRC Press, Boca Raton, Florida.

Sandau, K. and U. Hahn (1993) Some remarks on the accuracy of surface area estimation using the spatial grid. *J. Microscopy* **173**, 67–72.

Schneider, R. (1993) *Convex Bodies: The Brunn-Minkowski Theory.* Encyclopedia of Mathematics and Its Application, Vol. 44. Cambridge University Press, Cambridge.

Serra, J. (1969) *Introduction à la Morphologie Mathématique.* Cahiers du Centre de Morphologie Mathématique, Boolet No. 3, E.N.S.M.P.

Serra, J. (1982) *Image Analysis and Mathematical Morphology.* Vol. 1, Academic Press, London.

Widjajakususma, J., B. Biswal, and R. Hilfer (1999) Quantitative prediction of effective material properties of heterogeneous media. *Comp. Mat. Sci.*, in print.